Solid State Communications 197 (2014) 11–15

Contents lists available at ScienceDirect

Solid State Communications

journal homepage: www.elsevier.com/locate/ssc

Landau subband wave functions and chirality manifestation in rhombohedral graphite

Ching-Hong Ho [a], Cheng-Peng Chang [a,*], Ming-Fa Lin [b]

[a] Center for General Education, Tainan University of Technology, Tainan 710, Taiwan
[b] Department of Physics, National Cheng Kung University, Tainan 701, Taiwan

ARTICLE INFO

Article history:
Received 6 March 2014
Received in revised form
2 July 2014
Accepted 28 July 2014
by L. Brey
Available online 14 August 2014

Keywords:
A. Graphite
D. Chirality
D. Dirac cone
D. Landau level

ABSTRACT

Recently, rhombohedral graphite has been known to have a three-dimensional Dirac cone structure composed of tilted anisotropic Dirac cones, as a result of the perturbative interlayer electron hoppings. The corresponding Landau subbands have weak energy dispersions, a characteristic indicating the possible occurrence of a three-dimensional quantum Hall effect in weak magnetic fields. Since the robust zero-mode Landau subband should be topologically protected by the chirality of the Dirac fermions, here we investigate the chirality for rhombohedral graphite with regard to the Dirac cone tilt and anisotropy, for which there could exist phases mixing in the Landau subband wave functions. Both a perturbation analysis and an exact diagonalization are performed for showing the effects of the interlayer hoppings on the phases mixing. In the results the perturbations due to the interlayer hoppings are not resolvable. Rhombohedral graphite turns out to have the same chiral nature as monolayer graphene. The realizability of the three-dimensional quantum Hall effect in rhombohedral graphite is thus further supported by the manifestation of chiralities.

1. Introduction

The physics of Dirac cones in graphene gives new insight into the electronic properties of many condensed-matter systems. Besides the linear energy dispersion, there are 2-component wave functions in monolayer graphene (MG) due to the biparticle hexagonal lattice. A pseudospin degree of freedom arises [1], and thus the Dirac fermions are characterized by the chirality, i.e., the projection of the pseudospin on the direction of the momentum [2]. The Dirac fermions in MG exhibit opposite chiralities and acquire Berry's phase π around the two inequivalent Dirac points (DPs). The chiral symmetry is further carried in the corresponding Landau levels (LLs), of which the zero-mode LL is essential to the unconventional quantum Hall effect (QHE) realized in MG [3,4]. Such an electronic structure is altered when graphene layers are stacked and coupled. The massive Dirac fermions in bilayer graphene have different chiral nature and display another type of QHE [5]. In bulk graphite, a three-dimensional (3D) QHE with multiple plateaus has been observed [6]. It was ascribed to undoped rhombohedral (ABC-stacked) graphite (RG) or stacking faults (say, in ABABCBCB sequence) [7], which are usually found to be mixed with Bernal (AB-stacked) phase in natural graphite, as opposed to the theoretical demonstration of only one plateau for doped AB stacked graphite [8]. The ascription to RG can be further consolidated by a recently proposed 3D Dirac cone structure as follows [9].

RG is distinct from other stacks of graphene layers in that it has a biparticle bulk lattice belonging to the $R\bar{3}m$ space group, which is rhombohedral but not hexagonal [10,11]. In the dimensional crossover from ABC-stacked finite-layer graphene to RG, the bulk stack can be topologically nontrivial for the existence of surface states [11,12]. The bulk band in RG is described by the 3D Dirac cone structure that is composed of tilted anisotropic Dirac cones [9]. The lined-up Dirac points (DPs), dominated by the nearest interlayer tight-binding (TB) hopping, form two accidental band contact lines spiraling in opposite senses in the bulk dimension and surrounded by the famous sausage-link Fermi surface [13]. Within the minimal tight-binding (TB) model, which includes the nearest interlayer hopping only, all the Dirac cones along the DP spirals are equivalent to the normal ones realized in MG. The cone tilt and anisotropy are the consequences of the remaining interlayer hoppings, which serve as perturbations to the normal Dirac cones. Hence, the Landau subband (LS) energy dispersions in RG are much weaker than in AA- and AB-stacked graphites [14,15]; in attainable field strengths, only RG has multiple LS bulk gaps opened up as required for observing the 3D QHE.

* Corresponding author. Tel.: +886 6 2532106 5028.
E-mail address: t00252@mail.tut.edu.tw (C.-P. Chang).

http://dx.doi.org/10.1016/j.ssc.2014.07.022
0038-1098/

A deeper insight should be shed on the robustness of the zero-mode LS, which is essential to the 3D QHE. It is noted that in AA- and AB-stacked graphites the band contact lines are crucially supported by the crystal symmetries [16]; therefore, those band contact lines are not stable against impurities or crystal deformations. The corresponding zero-mode LSs are not ensured so that the 3D QHE is difficult to observe in those two types of graphite. It is well understood that, in general, the topological stability is related to the chirality. According to the index theorem [2], or in terms of explicit wave functions [17], the DPs of normal Dirac cones are topologically protected by the chiral symmetry. Within the first-order minimal model for RG, the DP spirals can be shown to be topologically stable, characterizing RG as a kind of 3D topological semimetal [12]; moreover, the 3D QHE can be described in terms of the chiral LL wave functions that are *a priori* casted for all the normal Dirac cones in the same way as for MG [7]. However, it is not so obvious that the chirality can be determined for an abnormal Dirac cone because the components of the LL wave function could be mixed. It seems unreasonable to presume the chiral nature for RG in view of the experimental finding of the 3D QHE [6], of which the origin might also be ascribed to stacking faults [7]. Thus, it is desirable to investigate the chiral nature of RG with respect to Dirac cone tilt and anisotropy beyond the minimal model. Indeed, tilted anisotropic Dirac cones also appear in deformed graphene or certain 2D organic metals [18], and the generalized chiral symmetry can be defined and shown to protect the zero-mode LL [19]. This communication is devoted to the LS wave functions and the chirality for RG. It is worthwhile to mention the recent experimental chirality manifestation for the Dirac cones in MG, which can be extended for 3D topological insulators such as Bi_2Se_3 and Bi_2Te_3 [20,21].

We start with an analysis of the low-energy LS wave functions in RG to show the perturbative effects of the interlayer hoppings. In an attempt to resolve the perturbations, an exact diagonalization is subsequently performed based on the magnetic translation symmetry, which provides a full-zone calculation and allows us to take into account all the interlayer hoppings. We adopt a non-primitive hexagonal unit cell to cope with the in-plane magnetic translation and consider the incommensurability between the hexagonal and the rhombohedral Brillouin zones (BZs). Our goal is to determine the effects of the interlayer hoppings on the phase mixing in the exactly obtained LS wave functions. The present method should be applicable to other rhombohedral systems, including certain 3D topological insulators where the phase mixing could be considerable.

2. 3D Dirac cone structure

The bulk lattice of RG is generated by the primitive unit vectors $\mathbf{a}_{1,2,3}$, which add up to a vector in the direction of the c-axis, as shown in Fig. 1(a). The primitive unit cell is embedded in a hexagonal cell with triple volume [10,11]. The biparticle lattice (A, B) in the periodic ABC-stacking configuration is decomposed into six sublattices (Al, Bl) as shown in Fig. 1(b), where $l(=1,2,3)$ is the layer label. The lattice constant of each sublattice is $a=2.46$ Å and the interlayer distance is $d=3.37$ Å. The relation of the first rhombohedral Brillouin zone (BZ) to the hexagonal BZ is illustrated in Fig. 2(a), a projection on a certain section defined by the coincident high-symmetry points of both BZs. We consider a nearest-neighbor TB model that includes interlayer hoppings up to next-adjacent layers. Referring to Fig. 1(b), the following hopping integrals are given: $\beta_0=-2.73$ eV, $\beta_1=0.32$ eV, $\beta_3=0.29$ eV, $\beta_4=0.15$ eV, $\beta_2=-0.0093$ eV and $\beta_5^{(\prime)}=0.0105$ eV [22].

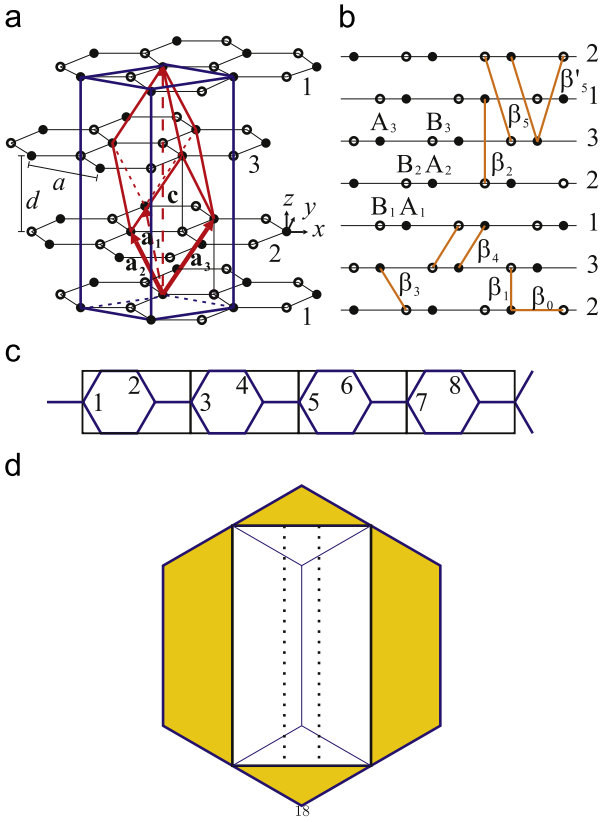

Fig. 1. (Color online) (a) Crystal lattice of RG, with the primitive rhombohedral cell (red) and the hexagonal cell (blue). (b) Periodic ABC stacks in bulk RG, within which the electron hoppings are indicated. (c) Schematic supercell with $m=4$. The $j(=1,2,\ldots,8)$th Sl atom ($S=A$, say) is labeled. (d) Illustration of folding from the 2D hexagonal BZ to a rectangular BZ and, further, to the magnetic BZ for the $m=4$ supercell.

The TB Bloch states are written as $|\psi_S\rangle_{\mathbf{k}}=N^{-1/2}\sum_{\mathbf{R}_S}\exp(i\mathbf{k}\cdot\mathbf{R}_S)|S\rangle$, with $\langle\mathbf{r}|S\rangle$ being the $2p_z$ atomic functions, $S=A,B$, where the summation runs over the N lattice points at $\mathbf{R}_S$ [13]. On this basis, the full-zone Hamiltonian matrix is written as

$$\mathcal{H}_{11}=\mathcal{H}_{22}=2\beta_4\,\Re\{f(k_x,k_y)\exp(-ik_z)\},$$

$$\mathcal{H}_{12}=\mathcal{H}_{21}^{*}=\beta_1\exp(ik_z)+\beta_0 f(k_x,k_y)+\beta_3 f^{*}(k_x,k_y)\exp(-ik_z), \qquad (1)$$

with the β_2 and $\beta_5^{(\prime)}$ hoppings being neglected, and $f(k_x,k_y)$ being the nearest-neighbor in-plane TB hopping amplitude. The low-energy band structure can be analyzed within the continuum approximation near the two edges of the hexagonal zone $(2\pi\xi/(\sqrt{3}a),2\pi\xi/(3a),k_z)$, $\xi=\pm1$ as specified in Fig. 2(b), where the 2D projections of the edges are denoted by $\overline{K}^{(\xi)}$. The in-plane wave vectors $(\kappa_x,\kappa_y)=(k_x,k_y)-\overline{K}^{(\xi)}$ are respectively defined with the κ_x axes directing from the edges $\overline{K}^{(\xi)}$ to the center line ($\overline{\Gamma}$) of the hexagonal zone [Fig. 2(b)]. The momentum phase $\vartheta_z=k_zd$ arises from the interlayer hoppings. We can thus derive the locations of the DPs, which are dominated by the β_1 hopping and have their coordinates off the edges at $\kappa_D=\beta_1(v_0\hbar)^{-1}[1+(v_3/v_0)\cos 3\vartheta_z]$ and $\vartheta_D=-\xi[\vartheta_z+(v_3/v_0)\sin 3\vartheta_z]$ [9,13], where v_0, v_3 and v_4 are the absolute values of β_0, β_3 and β_4 multiplied by $\sqrt{3}a/(2\hbar)$, respectively. These two DP spirals are found in the rhombohedral BZ from $-\pi/3d$ to $\pi/3d$ with opposite spiraling senses, as shown in Fig. 2(a). It is noted that, of the six DP spirals surrounding the six hexagonal edges, another two are found in the rhombohedral BZ from $-\pi/d$ to $-\pi/3d$, and the remaining two from $\pi/3d$ to π/d. The DP spirals are topologically stable as long as the space-time inversion symmetry of RG is not broken [12].